Corrosion Resistance of Two Niobium Containing Zirconium Alloy in Different Dissolved Hydrogen Concentration Primary Water Chemistry

Yunju Lee[a], Taeho Kim[a], Junhyuk Ham[a], and Ji Hyun Kim[a,*]
[a] *Department of Nuclear Engineering, School of Mechanical, Aerospace and Nuclear Engineering, Ulsan National Institute of Science and Technology, 50 UNIST-gil, Ulsan 44919*
[*] *Corresponding author: kimjh@unist.ac.kr*

1. Introduction

Zirconium alloys have been used for nuclear fuel cladding material of Pressurized Water Reactor(PWR), because they have a low thermal neutron cross section and reasonable mechanical properties. Recently, corrosion behavior of zirconium alloys has been intensively investigated due to burn-up extension of the nuclear reactors. Higher burnups may result in longer in-pile residence time that will increase corrosion.[1].

Thus, development of new zirconium alloy, which have higher corrosion resistance, become essential. From previous researches, it has been obvious that niobium addition on zirconium alloy gives great enhancement of the corrosion resistance of zirconium alloy. Recently, copper addition on niobium containing zirconium alloy shows enhancement in its corrosion behavior.

In waterside, corrosion of zirconium alloy proceeded to inward direction, from its surface to oxide-metal interface region. The oxygen ion propagated from water to metal region through oxygen vacancies in oxide region. Thus, the oxide property of zirconium alloy is the key for investigating the corrosion mechanism of zirconium alloys [2]. Recently, structure distribution of the zirconium alloy oxide is brought up as an indicator of the corrosion resistance of zirconium alloy. The zirconium alloy oxide is consisted of two distinct phases, tetragonal phase zirconium dioxide, and monoclinic phase zirconium dioxide. According to previous study, the tetragonal phase zirconium dioxide are usually found near oxide/metal interface, and monoclinic zirconium dioxide are distributed in upper region of zirconium oxide layer [2–4]. The tetragonal zirconium dioxide is usually formed in. With compressive stress in oxide layer, un-stoichiometric oxide and small grain size make the tetragonal phase zirconium dioxide is stabilized Because zirconium has relatively large Pilling-Bedworth ratio (about 1.56), strong compressive stress region exists near oxide-metal interface region. The compressive stress is released as the oxide layer grow up.

The dissolved hydrogen (DH) concentration is the key issue of primary water chemistry, and the effect of DH concentration on the corrosion rate of nickel based alloy has been researched. Recently, few researches were conducted to investigate the effect of DH concentration on corrosion resistance of zirconium alloy. However, the effect of DH on the zirconium alloy corrosion mechanism was not fully investigated.

In this work, Zr-Nb-Cu alloy and Zr-Nb-Sn alloy are oxidized at 360 °C of primary water for 20 d. Then, the high-resolution transmission electron microscopy (HR-TEM) is used to investigate the oxide growth of zirconium-water interface, the chemical composition of the specimens is also analyzed with energy-dispersed X-ray spectroscopy. The Raman spectroscopy was conducted to investigate structure of oxide layer. Each result is compared with the precedent study of author conducted in high DH concentration for same zirconium alloys. And the effect of DH concentration of water and different chemical composition of zirconium alloy on its oxide and the corrosion rate are studied.

2. Experimental

2.1. Specimen preparation

Two distinct types of zirconium alloys, Zr-Nb-Cu and Zr-Nb-Sn alloy plates were used for this research replicating the primary system of pressurized water reactor. The chemical compositions of two specimens are presented in Table 1. The specimen size of Zr-Nb-Sn is 10 mm × 8mm × 0.6 mm, and the specimen size for Zr-Nb-Cu is 10 mm × 5 mm × 0.75 mm, and they are polished before oxidization process. First, the SiC paper is used for grinding from 400 grit to 800 grit. Then, the polishing is conducted using 1 μm diamond paste. Finally, to minimize the mechanical deformation to zirconium alloy specimens, the 0.05 μm colloidal silica is used for polishing.

2.2 Procedure for corrosion experiment in simulated PWR water conditions

For this experiment, the polished Zr-Nb-Cu and Zr-Nb-Sn alloy plates were prepared. To simulate high temperature and high pressure the loop system with autoclave is utilized[4]. Using this simulating system, the primary water chemistry of PWR is set, temperature is 360 °C, pressure is 19 MPa, dissolved oxygen concentration is under 10 ppb, LiOH and H_3BO_3 concentration is 2 and 1200 ppm each. In this experiment, the two zirconium alloy plate specimens are oxidized in primary water chemistry for 20 d, and the DH concentration is maintained 30 cc/kg.

To characterize the microscale properties of oxide, the ex-situ investigation was conducted using JEOL JEM-2100F TEM in coincidence with EDS.

Table. 1 Chemical composition of Zr-Nb-Sn and Zr-Nb-Cu (in wt. %)

Alloy	Nb	Sn	Hf	Cu	C	O	N	Fe	Zr
Zr-Nb-Sn	0.96	0.76	0.002	-	0.1	0.62	0.03	0.18	Bal.
Zr-Nb-Cu	0.55	0.06	-	0.12	0.01	-	-	0.07	Bal.

The TEM samples were prepared by focused ion beam(FIB) milling method with a Quanta 3D Dual-Beam Focused Ion Beam attached to a field-emission gun scanning electron microscope (SEM). And to investigate the monoclinic phase zirconium oxide and tetragonal phase zirconium oxide in the oxide of the zirconium alloys ex-situ Raman spectroscopic measurement was performed on the surface of the specimens using Alpha300R with 532 nm wavelength ND: YAG laser in 10 mW power. And the laser penetration depth is considered to be ~1 μm.

3. Results and Discussion

3.1 HR-TEM analysis

The oxide properties of Zr-Nb-Sn alloy and Zr-Nb-Cu alloy in 360 °C of primary water for 20 d were characterized by TEM analysis. The scanning TEM images of (a) Zr-Nb-Cu alloy oxide and (b) Zr-Nb-Sn alloy oxide are shown in Fig. 1. From these images, the oxide thickness of each specimen is measured 10 times in equidistant interval, then average oxide thickness and standard deviation are appeared in Table. 2. For comparison, the results from precedent study which is conducted in high DH concentration is also appeared in Fig. 2. The average oxide thickness of Zr-Nb-Sn alloy is thicker than that of Zr-Nb-Cu alloy, which means that the corrosion resistance of Cu-containing zirconium alloy is better than that of Sn-containing zirconium alloy. These results are well matched with the precedent study and previous studies [5] conducted for Zr-Nb-Cu alloy. For both zirconium alloy, the oxide thickness of Zr-Nb-Cu alloy and Zr-Nb-Sn alloy were thicker at high DH concentration. This indicate that at high DH concentration, corrosion resistance of zirconium alloy decrease.

Table. 2 Measured oxide thickness from TEM image of two zirconium alloy specimens

[unit: μm]	Zr-Nb-Cu alloy	Zr-Nb-Sn alloy
30 cc/kg DH	0.799(0.069)	0.861(0.084)
50 cc/kg DH	1.30 (0.073)	1.45(0.063)

From Fig. 1, the difference of precipitates distribution between two specimens could be found. Zr-Nb-Cu alloy has larger number of smaller precipitates than Zr-Nb-Sn alloy. The result of point EDS analysis which is conducted for the bulk oxide and the precipitates is appeared in Table. 3, which shows that the precipitates are Nb-containing precipitate. Thus, it can be resulted that the Zr-Nb-Cu alloy has larger number of smaller niobium precipitates in its oxide than Zr-Nb-Sn alloy. These results are coincident with precedent study performed at high DH concentration and previous researches that conducted for copper and niobium containing zirconium alloys [5], which show that copper addition increases the number of relatively smaller niobium precipitates in Nb-containing zirconium alloy.

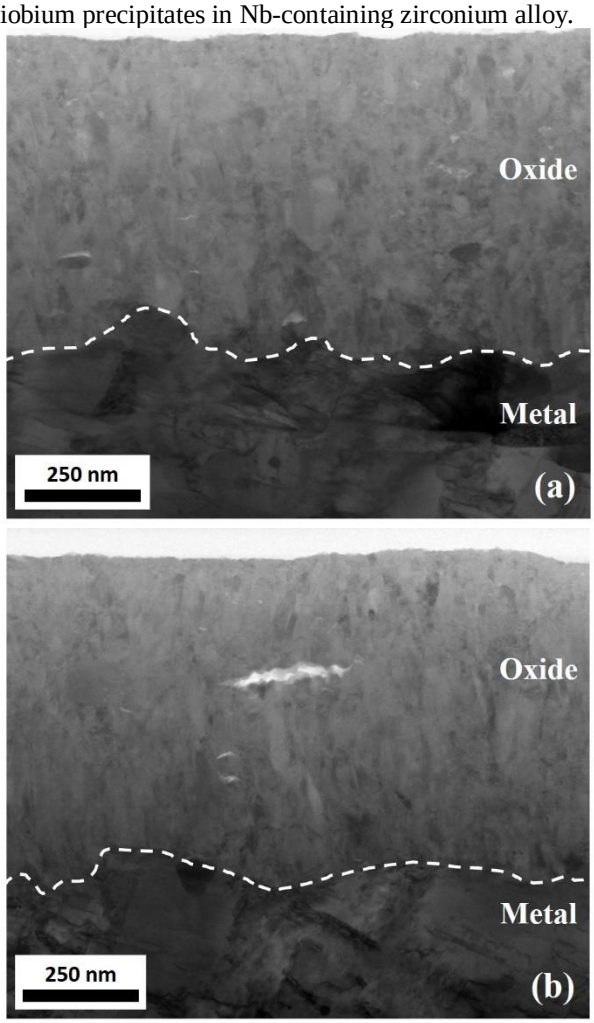

Fig. 1 STEM image of oxidized zirconium alloys in primary water chemistry. (a) Zr-Nb-Cu alloy and (b)Zr-Nb-Sn alloy

Table. 3 Point EDS results of the zirconium alloys in at. %

	Zr-Nb-Cu alloy		Zr-Nb-Sn alloy	
	Precipitate	Bulk	Precipitate	Bulk
O	7.54	16.61	62.55	65.88
Cu	34.45	70.54	-	-
Zr	6.71	12.85	21.02	32.26
Nb	31.29	0.0	14.87	0.70
Sn	0	0.0	1.56	1.16

From these results, the relationship between the copper concentration in Nb-containing zirconium alloy and its good corrosion resistance can be established. This

may result from the volume expansion during the phase transformation from tetragonal phase zirconium dioxide to monoclinic phase zirconium dioxide. According Qin et al. [3], the phase transformation from tetragonal phase zirconium dioxide to monoclinic phase zirconium dioxide is induced by compressive stress change. And it gives stress to oxide layer leading micro-cracking of bulk oxide and degrade the corrosion behavior of the zirconium alloy. Thus it is expected that the more niobium precipitates are distributed, the more tetragonal phase zirconium oxide exist [5], which means that the corrosion resistance of the zirconium alloy is better [2,5].

3.2 Raman spectroscopy

The oxide phase of Zr-Nb-Sn alloy and Zr-Nb-Cu alloy, which oxidized in 360 of PWR primary water condition and high DH concentration were investigated with Raman spectroscopy. The Raman spectrums of the two zirconium alloy surfaces which oxidized in 30 cc/kg of DH concentration is shown in Fig. 1 and the Raman peak position of the zirconium oxides are summarized in Table. 3. Because the beam penetration depth is larger than the oxide thickness of the zirconium alloys, the surface results can represent the whole oxide.

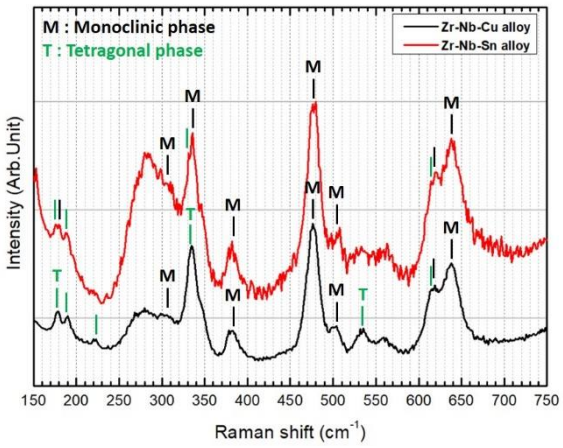

Fig. 1. Raman spectrum of Zr-Nb-Cu alloy surface (black line) and Zr-Nb-Sn alloy surface (red line) which are oxidized in 30 cc/kg of DH concentration.

Table. 3 Specification of Raman peak position obtained from the zirconium alloy oxidized in 30 cc/kg. [unit: cm^{-1}]

Zr-Nb-Cu		Zr-Nb-Sn	
Monoclinic	Tetragonal	Monoclinic	Tetragonal
-	179	180	179
-	189	-	189
-	232	-	-
307	-	307	-
337	332	337	332
382	-	382	-
476	-	476	-
502	536	502	-
617	615	617	615
638	-	638	-

The peaks located at 179 cm^{-1}, 189 cm^{-1}, 232 cm^{-1}, 332 cm^{-1}, 536 cm^{-1}, and 615 cm^{-1} are attributed to tetragonal phase zirconium dioxide and the peaks located at 180 cm^{-1}, 307 cm^{-1}, 337 cm^{-1}, 382 cm^{-1}, 476 cm^{-1}, 502 cm^{-1}, 617 cm^{-1}, and 638 cm^{-1} show monoclinic phase zirconium dioxide [6]. The Raman spectrum of the zirconium alloys oxidized in 30 cc/kg show larger number of tetragonal phase zirconium dioxide peak position in the Raman spectrum of Zr-Nb-Cu alloy than that of Zr-Nb-Sn alloy. And the peaks positioned at 332 cm^{-1} and 615 cm^{-1} show weaker peak intensity in the Raman spectrum of Zr-Nb-Sn alloy. The peaks which are attributed to monoclinic zirconium dioxide have strong intensity in Zr-Nb-Sn alloy than Zr-Nb-Cu alloy. These results refer that Zr-Nb-Cu alloy have higher fraction of tetragonal phase zirconium dioxide than Zr-Nb-Sn alloy.

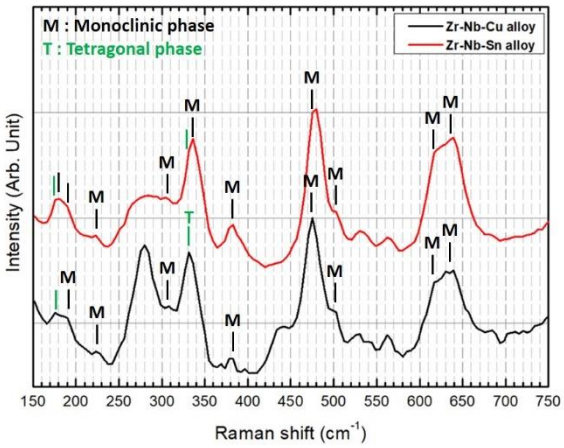

Fig. 1. Raman spectrum of Zr-Nb-Cu alloy surface (black line) and Zr-Nb-Sn alloy surface (red line) which are oxidized in 30 cc/kg of DH concentration.

Table. 4 Specification of Raman peak position obtained from the zirconium alloy oxidized in 50 cc/kg. [unit: cm^{-1}]

Zr-Nb-Cu		Zr-Nb-Sn	
Monoclinic	Tetragonal	Monoclinic	Tetragonal
-	179	180	179
190	-	190	-
232	-	232	-
307	-	307	-
-	332	337	332
382	-	382	-
476	-	476	-
502	-	502	-
617	-	617	-
638	-	638	-

Similar result is shown in the Raman spectrum of the zirconium alloy, which are oxidized in 50 cc/kg of DH concentration in Fig. 2. The peaks located at 179 cm^{-1} and 332 cm^{-1} represent the tetragonal phase zirconium dioxide and the peaks located at 180 cm^{-1}, 190 cm^{-1}, 307 cm^{-1}, 337 cm^{-1}, 382 cm^{-1}, 476 cm^{-1}, 502 cm^{-1}, 617 cm^{-1}, and 638 cm^{-1} indicated the monoclinic phase zirconium

dioxide. The Raman peak positions are summarized in Table.4. The peaks which indicate tetragonal phase zirconium dioxide show weaker intensity at Zr-Nb-Sn alloy than Zr-Nb-Cu alloy. And larger number of the monoclinic phase zirconium dioxide peak are shown in Zr-Nb-Sn alloy than Zr-Nb-Cu alloy.

The Raman spectroscopy of zirconium alloy, which oxidized at different DH concentration suggest same result that Zr-Nb-Cu alloy has higher fraction of tetragonal phase zirconium dioxide than Zr-Nb-Sn alloy. The results refer that the tetragonal-to-monoclinic phase transformation occur more often at Zr-Nb-Sn alloy oxide so that it shows lower fraction of tetragonal phase zirconium dioxide than Zr-Nb-Cu alloy. This is well matched with the oxidation results and HR-TEM results of the zirconium alloys that the more number of niobium precipitation exist, the higher tetragonal phase oxide fraction is.

In comparing the Raman spectrum of the zirconium alloys oxidized in 30 cc/kg of DH concentration and 50 cc/kg of DH concentration, the number of peak which attribute to tetragonal phase zirconium alloy are less at the zirconium alloy oxidized in high DH concentration. Also, for peak position, 190 cm^{-1}, 232 cm^{-1} which indicate monoclinic phase zirconium oxide shows higher intensity at the specimens oxidized at high DH concentration show smaller fraction of tetragonal phase zirconium oxide. This results apparently suggest that the corrosion resistance degradation at high DH concentration is related with the phase of oxide layer but, precise mechanism of degradation is not constructed.

4. Conclusion

In this study, HR-TEM analysis, and Raman spectroscopic measurement were conducted to investigate the effects of DH concentration and the chemical composition on the corrosion resistance and oxide phase of Zr-Nb-Cu alloy and Zr-Nb-Sn alloy after oxidizing in a primary water environment for 20 d. The corrosion rate of Zr-Nb-Cu alloy is slow, when it is compared to Zr-Nb-Sn alloy.

In TEM images, the oxide thickness of Zr-Nb-Cu alloy oxidized at 30 cc/kg of DH concentration was 0.799 μm and oxide thickness of Zr-Nb-Sn alloy, which also oxidized in same condition was 0.861 μm. Also, the niobium precipitates are distributed more densely in Zr-Nb-Cu alloy than Zr-Nb-Sn alloy. This phenomenon can be explained that the precipitate distribution affects compressive distribution in oxide layer. In comparing the results with precedent study of author which conducted in high DH concentration for same zirconium alloy, two specimens show same result that at high DH concentration the zirconium alloy shows degraded corrosion behavior.

From Raman spectrum of the zirconium alloys, Zr-Nb-Cu alloy has higher tetragonal zirconium oxide fraction than Zr-Nb-Sn alloy oxide. Due to compressive stress change, the tetragonal phase transform to monoclinic phase and this phase transformation gives stress to oxide layer making micro-crack and degrading the corrosion resistance of the zirconium alloy.

According to Raman spectroscopy results, the specimens oxidized at high DH concentration show smaller fraction of tetragonal phase zirconium oxide. It is obvious that the high DH concentration degrades the corrosion behavior of zirconium alloys but, the specific mechanism is not established.

ACKNOWLEDGEMENT

This work was financially supported by the International Collaborative Energy Technology R&D Program (No. 20168540000030) of the Korea Institute of Energy Technology Evaluation and Planning (KETEP) which is funded by the Ministry of Trade Industry and Energy, and the National Nuclear R&D program funded by Ministry of Science, ICT and Future Planning, and by the National Nuclear R&D program (NRF-2016M2B2A9A02944861) organized by the National Research Foundation (NRF) of South Korea in support of the Ministry of Science, ICT and Future Planning.

REFERENCES

[1] P. Rudling, R. Adamson, B. Cox, F. Garzarolli, A. Strasser, High burnup fuel issues, Nucl. Eng. Technol. 40 (2008) 1–8.

[2] J. Wei, P. Frankel, E. Polatidis, M. Blat, A. Ambard, R.J. Comstock, L. Hallstadius, D. Hudson, G.D.W. Smith, C.R.M. Grovenor, M. Klaus, R.A. Cottis, S. Lyon, M. Preuss, The effect of Sn on autoclave corrosion performance and corrosion mechanisms in Zr-Sn-Nb alloys, Acta Mater. 61 (2013) 4200–4214.

[3] W. Qin, C. Nam, H.L. Li, J.A. Szpunar, Tetragonal phase stability in ZrO 2 film formed on zirconium alloys and its effects on corrosion resistance, 55 (2007) 1695–1701.

[4] T. Kim, J. Kim, K.J. Choi, S.C. Yoo, S. Kim, J.H. Kim, Phase transformation of oxide film in zirconium alloy in high temperature hydrogenated water, Corros. Sci. 99 (2015) 134–144.

[5] J.-Y. Park, B.-K. Choi, S.J. Yoo, Y.H. Jeong, Corrosion behavior and oxide properties of Zr–1.1wt%Nb–0.05wt%Cu alloy, J. Nucl. Mater. 359 (2006) 59–68.

[6] J.E. Maslar, W.S. Hurst, W.J. Bowers, J.H. Hendricks, In situ Raman spectroscopic investigation of zirconium-niobium alloy corrosion under hydrothermal conditions, J. Nucl. Mater. 298 (2001) 239–247.